Research Article Vol. 29, No. 13 / 21 June 2021 / Optics Express 19515
Optics EXPRESS

Accuracy enhanced microwave frequency measurement based on the machine learning technique

DIFEI SHI,[1,2,3,4] GUANGYI LI,[1,2,3,4] ZHIYAO JIA,[1,2,3] JUN WEN,[1,2,3] MING LI,[1,2,3] NINGHUA ZHU,[1,2,3] AND WEI LI[1,2,3,*]

[1]State Key Laboratory on Integrated Optoelectronics, Institute of Semiconductors, Chinese Academy of Sciences, Beijing 100083, China
[2]School of Electronic, Electrical and Communication Engineering, University of Chinese Academy of Sciences, Beijing 100049, China
[3]Center of Materials Science and Optoelectronics Engineering, University of Chinese Academy of Sciences, Beijing 100190, China
[4]These authors contributed equally to this work
[*]liwei05@semi.ac.cn

Abstract: We propose and experimentally demonstrate a microwave frequency measurement system based on the photonic technique. An amplitude comparison function is constructed to perform frequency-to-power mapping based on a non-sliced broadband optical source. The results are fed into a machine learning module which can be utilized to minimize the differential mode noise of the system caused by the polarization fluctuation. The system is reconfigurable with adjustable measurement bandwidth by adjusting the dispersion group delay of the signals at orthogonal polarizations by a polarization division multiplexed emulator (PDME). In addition, the mapping relationship is reconstructed by stacking method. The results are fed into four machine learning models: support vector regressor (SVR), KNeighbors regressor (KNN), polynomial regressor (PR) and random forest regressor (RFR). The output of the four models then combined by adding them together using linear regression method. By fitting the relationship between frequency and microwave power ratio with machine learning method, the accuracy of microwave frequency measurement system is further improved. The results show that for a measurement system with a bandwidth of 2 GHz and 4 GHz, the maximum error and the average measurement errors are all reduced. The results are promising for applications of modern radar and electronic warfare systems.

1. Introduction

Microwave frequency estimation plays an important rule for modern radar and electronic warfare systems. As electronic systems develop towards much higher bandwidth and abundant spectral bands, microwave frequency measurement system with larger bandwidth and good reconfigurability is highly demanded. However, for modern electronic technology-based measurement systems, it is hard to exceed 18 GHz [1]. Moreover, they are generally electromagnetic sensitive. Photonic based microwave measurement systems have been extensively studied to overcome the drawbacks. Generally, photonic based frequency estimation methods are realized by mapping the frequency information to some parameters which can be captured more conveniently, such as pulse time [2,3], spatial information [4,5] and microwave power [6–9] of the signals.

For frequency-to-time mapping, the unknown frequency components are separated on time domain. The relationship between the frequency and time information can be established by micro-ring resonator [2] and Fourier domain mode lock lasers [3]. The frequency-to-time mapping schemes is capable of measuring multiple signals. However, the real-time performance is not satisfactory. For frequency-to-space mapping, microwave signals with different frequency

#429904 https://doi.org/10.1364/OE.429904
Journal © 2021 Received 27 Apr 2021; revised 26 May 2021; accepted 1 Jun 2021; published 8 Jun 2021

Optics EXPRESS

components are separated in spatial channels by means of a spatial filter such as a Bragg grating Fabry-Perot device [4] or a diffraction grating [5]. Theoretically, the accuracy can be improved by adding more channels. Whereas, this would in turn induce more cost and complexity to the system.

For frequency-to-power mapping technology, a relationship is constructed between unknown microwave frequency and microwave [6–10] or optical power [11]. An amplitude comparison function is established by constructing two different frequency-amplitude functions. Amplitude comparison functions (ACFs) can be generated by dispersion induced power fading functions [6–8], and microwave photonic filters [9]. In [6], we demonstrated a reconfigurable IFM system with a measurement bandwidth of 12 GHz based on stimulated Brillouin scattering, Whereas, temperature control is required for practical applications since SBS effect is sensitive to temperature variation. In [8], microwave frequency estimation with a measurement range of 8 GHz is performed. However, the measurement range can be adjusted with limited bandwidth due to the relatively small dispersion caused by wavelength tuning. Recently, we proposed a reconfigurable photonic frequency measurement system based on microwave photonic filters technique [10]. Thanks to the construction of ACF, common-mode noise is suppressed, leading to a power independent system. However, in our work, multiple optical paths are induced, the power fluctuation of a single frequency-amplitude function will be induced due to the jitter of the separated optical paths, which may degrade the performance of the systems.

In this paper, we propose and experimentally demonstrate a reconfigurable instantaneous frequency measurement (IFM) system with improved accuracy based on machine learning technique. Frequency-to-power mapping scheme are performed by a non-sliced broadband optical source. And the system is reconfigurable by simply adjusting the polarization division multiplexing emulator (PDME). Also, the system is more stable thanks to the reduced number of optical paths. More importantly, a stacking regression method is applied to further induced to reduce the measurement errors of the system. Machine learning and deep learning techniques have been widely applied in optoelectronic fields to enhance the performance of the systems. In [12], convolution neural network (CNN) is applied to optimize a Brillouin assisted measurement system. However, digital signal processing is required before the CNN process. Also, a deep neural network (DNN) is utilized to improve the performance of a frequency-to-time mapping scheme [13]. Different from the aforementioned works, a stacking regressor is applied to an IFM system which combine multiple regression models via a meta-regressor. Large number of ACFs are collected and fed into the machine learning algorithm, by utilizing regression methods, an optimized ACF can be constructed which has a better resistance for the power fluctuation of the system. In addition, the superiority of multiple regressors can be combined and the performance of the system can be further improved.

2. Principle

The schematic diagram of the proposed IFM system is shown in Fig. 1. Figure 1(a) shows the configuration of the proposed IFM system. Firstly, a broadband optical source (BOS) is shaped by a waveshaper (WS). Afterwards, the shaped optical signal is adjusted by a polarization controller (PC1) and injected into a dual-polarization dual-drive Mach-Zehnder modulator (DPol-DDMZM). The DPol-DDMZM consists of two dual-drive Mach-Zehnder modulators and a 90° polarization rotator, which allows the generation of two orthogonal modulated optical signals. The signals at the upper DDMZM are phase-modulated by the unknown signals, while the optical signals at the lower DDMZM pass through the modulator directly. Afterwards, a polarization division multiplexed emulator (PDME) is utilized to induce a tunable dispersion group delay (DGD) after aligning its principle axes with the polarization states of optical signals through a polarization controller (PC2). The optical signals are then separated by an optical coupler (OC). The signals at the upper path is combined by a polarizer (Pol1) aligned at 45° to the principle axis of the PDME.

Optics EXPRESS

After passing through the dispersion element (DE) and the two optical circulators, the signals at the upper path are detected by PD2. It is noted that given the incoherence of the frequency components of the BOS, the transfer function of the sub-system can be seen as the accumulation of the optical frequency components and the corresponding modulated sidebands. According to our previous work [10], the transfer function can be expressed as:

$$\begin{aligned} H_{\mathrm{RF1}}(\omega) \propto & \frac{m}{2}\exp[\mathrm{j}(\Omega_0\Delta\tau_1 - \frac{\beta_2\omega^2}{2})]H_{\mathrm{b}}(\omega-\omega_{\mathrm{c1}}) \\ & + \frac{m}{2}\exp[\mathrm{j}(-\Omega_0\Delta\tau_1 + \frac{\beta_2\omega^2}{2})]H_{\mathrm{b}}(\omega+\omega_{\mathrm{c1}}), \end{aligned} \tag{1}$$

where Ω_0 is the center frequency of the BOS source, $\Delta\tau_1$ is the DGD induced by the PDME, β_2 is the dispersion induced by the DE. The optical frequency of the BOS is donated as Ω. ω_{c} is the center frequency of the transfer function which can be expressed as $\omega_{\mathrm{c1}} = \Delta\tau_1/\beta_2$. $H_{\mathrm{b}}(\omega)$ is the baseband response which is given by [14]:

$$H_{\mathrm{b}}(\omega) = \int_0^{\infty} N(\Omega)e^{-j\beta_2(\Omega-\Omega_0)\omega}d\Omega. \tag{2}$$

where $N(\Omega)$ is the power spectral density. The optical signal at the lower branch is adjusted by a PC3 and pass through a polarization maintaining fiber (PMF). Based on the same principle, a DGD is further induced to the orthogonal optical signals at the lower branch. Thus, the transfer function of the lower branch is shown as:

$$\begin{aligned} H_{\mathrm{RF2}}(\omega) \propto & \frac{m}{2}\exp[\mathrm{j}(\Omega_0\Delta\tau_2 - \frac{\beta_2\omega^2}{2})]H_{\mathrm{b}}(\omega-\omega_{\mathrm{c2}}) \\ & + \frac{m}{2}\exp[\mathrm{j}(-\Omega_0\Delta\tau_2 + \frac{\beta_2\omega^2}{2})]H_{\mathrm{b}}(\omega+\omega_{\mathrm{c2}}), \end{aligned} \tag{3}$$

where m is a strength factor, $\Delta\tau_2 = \Delta\tau_1 + \Delta\tau$. $\Delta\tau$ is the DGD induced by the PMF. $\omega_{\mathrm{c2}} = \Delta\tau_2/\beta_2$. It should be noted that the negative part of the transfer function makes far less contribution than the positive parts. Thus, the negative part is ignored. The transfer functions given by Eq. (1) and Eq. (3) can be regarded as two filters. If a Gaussian shaped WS with an overall bandwidth of w_{N} is utilized, the amplitude comparison function can be expressed as:

$$\gamma_{\mathrm{sq}} = \frac{|H_{\mathrm{filter1}}(\omega-\omega_{c1})|}{|H_{\mathrm{filter2}}(\omega-\omega_{c2})|} \propto \frac{\exp[-\frac{4\ln 2(\omega-\omega_{c1})^2}{\omega_{\mathrm{3dB}}}]}{\exp[-\frac{4\ln 2(\omega-\omega_{c2})^2}{\omega_{\mathrm{3dB}}}]}, \tag{4}$$

where ω_{3dB} is the 3dB bandwidth of the transfer function which is given by:

$$\omega_{\mathrm{3dB}} = \frac{\sqrt{8\ln 2}}{\beta_2 W_N}. \tag{5}$$

From the Eq. (4), the amplitude comparison function is constructed by the two MPFs. By dividing the two transfer functions, the power fluctuation of the system can be effectively eliminated. Therefore, the proposed system is immune to the power fluctuation of unknown RF signals. In addition, the center frequencies and bandwidth of the two filters determine the measurement range and bandwidth of the IFM system, which can be increased by introducing more time delay via PDME and adjusting the WS.

Afterwards, the measured ACFs are fed into the machine learning model for regression. The machine learning model is a stacking regressor consist of two layers. The first layer consists of four regressors: support vector regressor (SVR), KNeighbors regressor (KNN), polynomial regressor (PR) and random forest regressor (RFR).

Optics EXPRESS

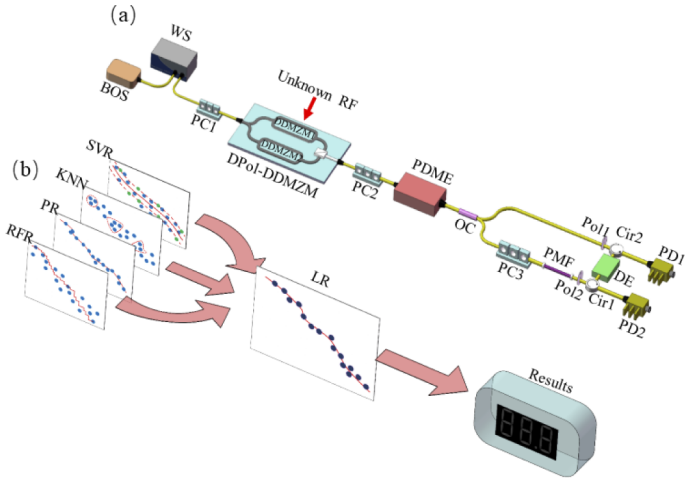

Fig. 1. Schematic configuration of (a) the proposed IFM system and (b) stacking regressor. BOS: broadband optical source; WS: waveshaper; PC: polarization controller; DPol-DDMZM: dual-polarization dual-drive Mach-Zehnder modulator; PDME: polarization division multiplexing emulator; OC; optical coupler; PMF: polarization maintaining fiber; Pol: polarizer; Cir: circulator; DE: dispersion element; PD: photodetector; SVR: support vector regressor; KNN: KNeighbors Regressor; PR: polynomial regressor; RFR: random forest regressor; LR: linear regressor.

SVR is a supervised machine learning algorithm which is widely applicable for numerical parameters prediction [15]. Assuming A_{ACF} is the result of the measured power ratio. The main equation for SVR is a linear regression equation which can be expressed as

$$pre(A_{\mathrm{ACF}})_{\mathrm{SVR}} = WA_{\mathrm{ACF}} + b, \tag{6}$$

where $pre(A_{\mathrm{ACF}})_{\mathrm{SVR}}$ is the predict microwave frequency for SVR, W is the weight parameter, and b is the bias. The parameters can be optimized based on the following process, which is given by

$$\begin{aligned} &\min \tfrac{1}{2}||W||^2 + C\sum_{i=1}^{N}(\xi_{\mathrm{i}} + \xi_{\mathrm{i}}^*) \\ &\text{subject to} \begin{cases} pre(A_{\mathrm{ACF}}) - WA_{\mathrm{ACF}} - b \ \le \varepsilon + \xi_{\mathrm{i}} \\ WA_{\mathrm{ACF}} + b - y_{\mathrm{i}} \ \le \varepsilon + \xi_i^* \\ \xi_{\mathrm{i}}, \xi_i^* \ \ge 0 \end{cases} \end{aligned} \tag{7}$$

where C is the regularization term, ξi, ξi^* are sets of non-negative slack variables which permits a certain violation of the ε-tube's bounds. However, it should be noted that a linear model usually cannot fulfill practical feasibilities. Thus, a Kernel function is added to convert the linear function to a nonlinear function. The input variable of i order is set to be A_{ACFi}, the nonlinear function can thus be expressed as

$$pre(A_{\mathrm{ACF}})_{\mathrm{SVR}} = WK(A_{\mathrm{ACF}}, A_{\mathrm{ACFi}}) + b, \tag{8}$$

Gaussian kernel with simple mathematical representation is more appropriately utilized in our experiment since the usage of Gaussian kernel spares the computation memory. Also, the Gaussian kernel utilized in the system can fulfill the needs for frequency estimation, which can

Optics EXPRESS

be seen in the experimental part. For the microwave photonic based IFM system, a Gaussian kernel is utilized to optimize the ACF which can be expressed as

$$K(A_{\mathrm{ACF}}, A_{\mathrm{ACFi}}) = \exp(-\frac{|A_{\mathrm{ACF}} - A_{\mathrm{ACFi}}|^2}{2\gamma^2}). \tag{9}$$

γ is a parameter to determine the property of the kernel function.

KNN is a simple and compact algorithm. The frequency measurement result is predicted by local interpolation of the targets related to the k nearest results of the training set [16]. Generally, the distance between the training and testing sets can be expressed as

$$dist(pre(A_{\mathrm{ACF}})_{\mathrm{KNN}}, tra(A_{\mathrm{ACFi}})_{\mathrm{KNN}}) = (|pre(A_{\mathrm{ACF}})_{\mathrm{KNN}} - tra(A_{\mathrm{ACFi}})_{\mathrm{KNN}}|^p)^{\frac{1}{p}}, \tag{10}$$

where A_{ACFi} is the amplitude comparison function of the training data for KNN algorithm. p is a parameter which determines which kind of distance should be utilized. Euclidean distance brings more convenience and higher accuracy after comparison in our post-processing. Therefore, the parameter p is set to 2, which corresponds to Euclidean distance. Also, it should be noted that since stacking regression is employed, the four estimators at the first layer share the same training dataset, i.e. A_{ACFi}.

For polynomial regression, the output signal is a nth degree polynomial to the input signal, which is given by [17]

$$pre(A_{\mathrm{ACF}})_{\mathrm{PR}} = \theta_{\mathrm{n}} {A_{\mathrm{ACF}}}^{\mathrm{n}} + \theta_{\mathrm{n-1}} {A_{\mathrm{ACF}}}^{\mathrm{n-1}} + \ldots + \theta_0 = \sum_{j=0}^{n} \theta_{\mathrm{j}} {A_{\mathrm{ACF}}}^{\mathrm{j}}, \tag{11}$$

where θ_{n} is the nth order of polynomial. And the corresponding loss function is given by

$$J(\theta)_{\mathrm{PR}} = \frac{1}{2m}\{[\sum_{i=1}^{m} (pre(A_{\mathrm{ACF}})_{\mathrm{PR}} - tra(A_{\mathrm{ACFi}})_{\mathrm{PR}}]^2 + \lambda \sum_{i=1}^{N} |\theta_i^2|\}, \tag{12}$$

where $tra(A_{\mathrm{ACF1}})$ is the training dataset. And λ is the regularized parameter of the L2 regularizer, which is induced to avoid overfitting.

RFR is an improved regression method which is robust and flexible for constructing a relationship between the input function and the output results [18]. The RFR consists of a collection of regression trees, which use different bootstraps of training data for the regression process. Each tree works as one regressor and the final output is calculated to be the average output of the individual regression trees. By adding proper number of trees to the RFR, overfitting can be effectively avoided.

Finally, the output of the four estimators at the first layer is summed up using LR, which can be shown as [19]

$$pre(A_{\mathrm{ACF}})_{\mathrm{final}} = c_1 pre(A_{\mathrm{ACF}})_{\mathrm{SVR}} + c_2 pre(A_{\mathrm{ACF}})_{\mathrm{KNN}} + c_3 pre(A_{\mathrm{ACF}})_{\mathrm{PR}} + c_4 pre(A_{\mathrm{ACF}})_{\mathrm{RFR}} \tag{13}$$

c_{n} is the weighting parameters corresponding to the four algorithms. By utilizing the stacking method, the results of the multiple estimators are combined. An optimized ACF can be constructed and the accuracy of the frequency measurement system can be enhanced.

3. Experimental results

A proof-of-concept experiment based on the setup shown in Fig. 1 was carried out. A BOS was shaped by a rectangular WS which centered at 1549.91 nm with a 3-dB bandwidth of about 600 pm. After passing through an EDFA and a polarization controller (PC), the optical signal is

Optics EXPRESS

injected into a DPol-DDMZM. By utilizing phase modulation, transfer functions with monotonic slope can be realized, which allow the measurement of unknown microwave frequencies at specific frequency ranges. During the experiment, the power of the BOS is set to be 10 dBm. And the dispersion medium during the experiment is a dispersion compensation fiber (DCF) with a dispersion of 450 ps/nm. Thanks to the two polarization circulators, only one roll of DCF is needed during the experiment. The power functions of the proposed system are captured by a vector network analyzer (VNA). The output power of the continuous-wave electrical signal from the VNA was set to 10 dBm.

Firstly, a PMF which induces a time delay of about 7 ps for orthogonal polarizations is utilized. Also, the PDME is tuned to induce a time delay of 14 ps for the two polarizations. Under this circumstance, transfer functions with the center frequencies of 4 GHz and 6 GHz can be generated, which allow the measurement for an unknown microwave signal with a frequency range of 4–6 GHz. Figures 2(a-i) and 2(a-ii) show the monotonic transfer functions, and five groups of ACFs are given. It can be seen from Fig. 2(b-i) that due to the differential noise, fluctuation is induced which may lower the accuracy of the proposed system. During the experiment, we randomly select one ACF for microwave frequency estimation and 45 frequencies are selected as unknown frequencies. Figure 2(c-i) shows the results, as can be seen, the average error for frequencies within 4–6 GHz is about 47.5 MHz. And the maximum measurement error is 143 MHz. To further improve the accuracy, stacking regressor is induced and 40 groups of ACFs are fed into the machine learning algorithm. The stacking regressor consists of two layers, the first layer consists of 4 algorithms, the RFR, the KNN regressor, the PR and SVR. RFR is robust to overfitting since the generalization error of the model is convergent by adding more trees [20]. During the experiment, 300 estimators are utilized. 10 neighbors are selected for KNN. For the support vector regressor, epsilon is set to be 0.0001 and C is set to be 4×10^7. For the polynomial regressor, the degree is set to be 40 and alpha is set to be 0.001, L2 regularizer are utilized to prevent overfitting. The second layer is a linear regressor module which combines the results of the first layer together. For each measurement procedure, 50 groups of ACFs are constructed. 80 percent of the dataset is utilized to train the machine learning algorithm and 20 percent are utilized to test the machine learning module. The optimized ACF can be seen in Fig. 2(b-ii). Also, 45 microwave frequencies are measured and the results are shown in Fig. 2(c-ii). The maximum error is 100 MHz and the average measurement error is measured to be 35 MHz.

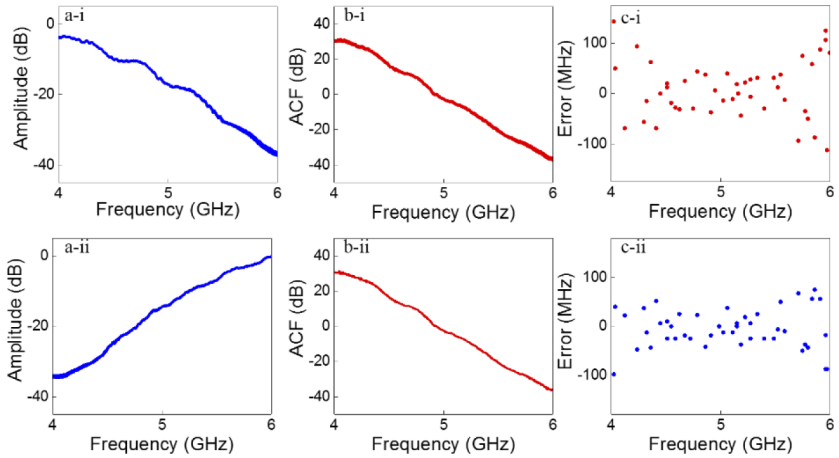

Fig. 2. Measured frequency response with the frequency range of 4–6 GHz with (a-i) a monotonic decreasing slope and (a-ii) a monotonic increasing slope. (b-i) The corresponding 5 group ACFs and (b-ii) the optimized ACF. The measurement results for (c-i) the unoptimized ACF and (c-ii) the optimized ACF.

Optics EXPRESS

Moreover, it is noted that the frequency measurement system is reconfigurable with adjustable measurement ranges. The length of the PMF is fixed and the PDME is tuned to induce a time delay of about 38 ps. In this case, the center frequencies of the transfer functions are tuned to be 11 GHz and 13 GHz. Figures 3(a-i), (a-ii) and (b-i) show the monotonic transfer functions and the corresponding ACFs. Based on a same measurement method, an ACF is randomly chosen. Figure 3(c-i) shows the measurement results. A maximum measurement error of 87 MHz and an average measurement error of 40 MHz is realized. Further, 40 groups of ACFs are fed into the machine learning algorithm and the optimized ACF is shown in Fig. 2(b-ii). 45 microwave frequencies are measured. A maximum measurement error of 62 MHz and an average measurement error of about 32 MHz is realized, which is shown in Fig. 3(c-ii).

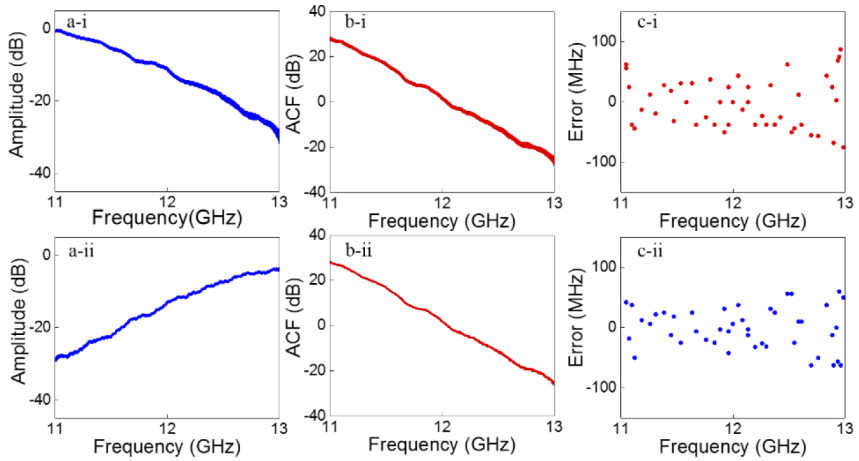

Fig. 3. Measured frequency response with the frequency range of 11–13 GHz with (a-i) a monotonic decreasing slope and (a-ii) a monotonic increasing slope. (b-i) The corresponding 5 group ACFs and (b-ii) the optimized ACF. The measurement results for (c-i) the unoptimized ACF and (c-ii) the optimized ACF.

In addition, the measurement system is reconfigurable for adjustable measurement bandwidth. The 3-dB bandwidth of the BOS is narrowed to be about 300 pm. Under this circumstance, a PMF which induces a relative time delay of 14 ps for the two polarizations is induced. Firstly, the PDME is adjusted to induce a time delay of 14 ps. Transfer functions with the center frequencies of 4 GHz and 8 GHz are generated, as is shown in Figs. 4(a-i) and 4(a-ii). Thus, unknown microwave frequency within the range of 4–8 GHz can be estimated. Figure 4(b-i) illustrate the constructed 5 groups of ACFs by subtracting the two transfer functions. We randomly select one ACF to measure the unknown microwave frequencies. 65 unknown microwave signals are measured and the maximum measurement error is 150 MHz and the average measurement error is about 38 MHz. The results can be seen in Fig. 4(c-i). Forty groups ACFs are fed into the machine learning algorithm and the optimized ACF is shown in Fig. 4(b-ii). Also, 65 unknown microwave signals are measured and the maximum measurement error is 100 MHz. As shown in Fig. 4(c-ii), the average measurement error is about 33 MHz. The accuracy of the proposed microwave measurement system is improved.

Finally, the PDME is adjusted to induce a time delay of 28 ps for the orthogonal polarizations. Microwave photonic power functions centered at of 8 GHz and 12 GHz are realized, which are shown in Figs. 5(a-i) and 5(a-ii). The corresponding ACFs and the optimized ACF can be seen in Figs. 5(b-i) and 5(b-ii). Figures 5(c-i) and 5(c-ii) show the measurement results. As can be seen, a maximum measurement error of 150 MHz and an average measurement error of 44 MHz are realized for the unoptimized ACF. For the optimized ACF, a maximum measurement error of 93

Optics EXPRESS

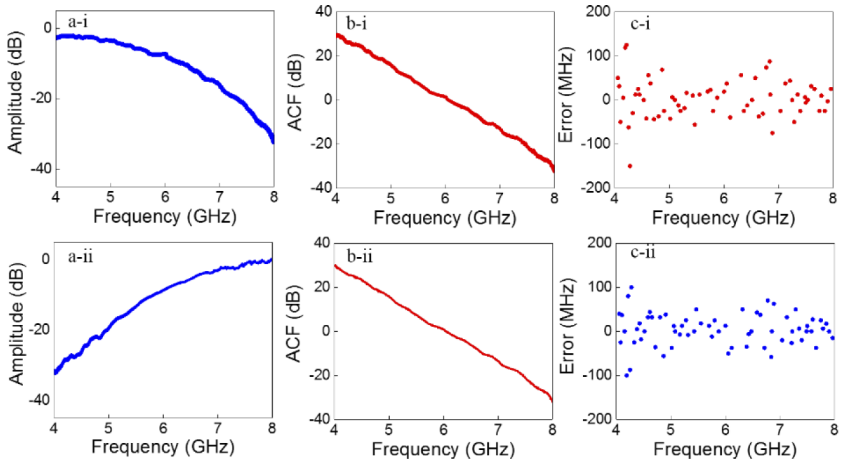

Fig. 4. Measured frequency response with the frequency range of 4–8 GHz with (a-i) a monotonic decreasing slope and (a-ii) a monotonic increasing slope. (b-i) The corresponding 5 group ACFs and (b-ii) the optimized ACF. The measurement results for (c-i) the unoptimized ACF and (c-ii) the optimized ACF.

MHz and an average measurement error of about 34 MHz are realized. By utilizing machine learning method, the differential noise caused by the polarization fluctuation is successfully suppressed.

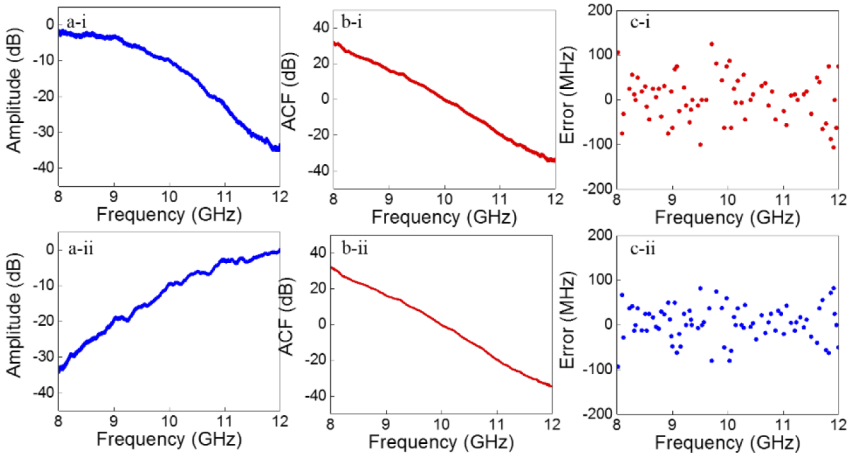

Fig. 5. Measured frequency response with the frequency range of 8–12 GHz with (a-i) a monotonic decreasing slope and (a-ii) a monotonic increasing slope. (b-i) The corresponding 5 group ACFs and (b-ii) the optimized ACF. The measurement results for (c-i) the unoptimized ACF and (c-ii) the optimized ACF.

Moreover, in order to show the noise performance and the nonlinear distortion of the proposed IFM system, the spurious-free dynamic range (SFDR) was examined by using two-tone modulation. During the experimental measurement process, two tone signals with the frequencies of 4.2 GHz and 4.205 GHz are measured. The measured results are shown is Fig. 6. The SFDR of the proposed IFM system is measured to be 79.0 dB $\cdot$ $Hz^{2/3}$ at a noise floor of -118.5 dBm/Hz. The 3-dB compression point was calculated to be 22.5 dBm.

Optics EXPRESS

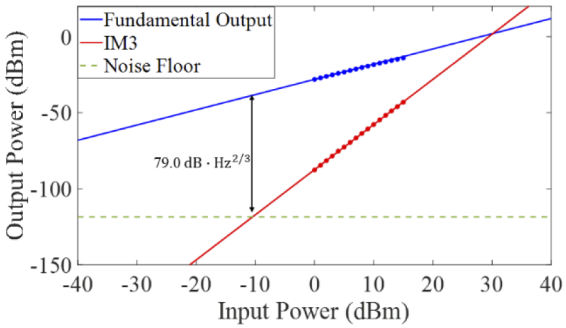

Fig. 6. Measured power of the fundamental and third-order intermodulation distortion components versus the input RF power.

Also, it is noted that by narrowing the bandwidth of the BOS, the bandwidth of the IFM system can be further improved [9]. Whereas, under this circumstance, the optical signal before the EDFA will decrease and under this circumstance, the EDFA in the system would induce more gain for the optical source, and the noise will increase, which will degrade the performance of the frequency measurement system. Also, the EDFA has a threshold for the input power. Thus, only measurement processes with the bandwidth of 2 GHz and 4 GHz were performed.

In addition, it is worth noting that the latency of the system is mainly induced by the 4 km DCF in the system. The DCF with a second-order dispersion of β_2 is modeled as a phase filter in our scheme which is used to induce different time delays of the frequency components of the BOS. However, it is noted that a linear-chirp fiber Bragg grating [21] is able to emulate the same dispersion, which will make the system more compact and the time delay performance will be improved. Moreover, it is noted that same estimator has different performance on different curves. For the measurement range of 4–6 GHz, the RFR gives the best performance with an average error of 31.5 MHz. For the measurement range of 11 GHz-13 GHz, the PR gives the best performance with an average measurement error of about 28 MHz. For the measurement range of 4 GHz-8 GHz, also, the RFR gives the best performance with an average measurement error of 31.2 MHz. Finally, for the frequency estimation process of 8 GHz-12 GHz, the KNN gives the best estimation performance of an average error of 30.8 MHz. Moreover, the LR model after the four regressions are added to further fit the ACF curve and increase the accuracy. The weights of the four regressors are assigned based on their accuracy. The higher the accuracy is, the higher the weight will be. Thus, stacking learning method was utilized in our post-processing.

As for the repeatability of the proposed system, our system is mainly affected by the polarization elements of the system, such as the PC, PDME and PMF. Therefore, the proposed configuration is sensitive to the precise control of polarization. By utilizing machine learning method, the differential noise caused by the polarization fluctuation is successfully suppressed. In addition, a polarization state monitor can further be utilized to guarantee the polarization stability of the system in real-world applications.

4. Conclusion

In conclusion, a photonic assisted IFM system is proposed and experimentally demonstrated. Reconfigurable transfer functions are constructed by non-sliced BOS. The IFM system is reconfigurable with adjustable measurement range and bandwidth. More importantly, by using machine learning technique, the differential noise of the system caused by polarization fluctuation is suppressed, leading to a more precise frequency estimation system, which is a potential solution for frequency estimation for electronic warfare systems.

Optics EXPRESS

Funding. National Natural Science Foundation of China (60620106013, 61431003, 61535012, 61835010).

Disclosures. The authors declare no conflicts of interest.

Data availability. Data underlying the results presented in this paper are not publicly available at this time but may be obtained from the authors upon reasonable request.

References

1. J. Yao, "Microwave Photonics," J. Lightwave Technol. **27**(3), 314–335 (2009).
2. F. Zhou, H. Chen, X. Wang, L. Zhou, J. Dong, and X. Zhang, "Photonic multiple microwave frequency measurement based on frequency-to-time mapping," IEEE Photonics J. **10**(2), 1–7 (2018).
3. T. Hao, J. Tang, W. Li, N. Zhu, and M. Li, "Microwave photonics frequency-to-time mapping based on a fourier domain mode locked optoelectronic oscillator," Opt. Express **26**(26), 33582–33591 (2018).
4. S. T. Winnall, A. C. Lindsay, M. W. Austin, J. Canning, and A. Mitchell, "A microwave channelizer and spectroscope based on an integrated optical Bragg-grating Fabry-Perot and integrated hybrid fresnel lens system," IEEE Trans. Microwave Theory Tech. **54**(2), 868–872 (2006).
5. W. Wang, R. L. Davis, T. J. Jung, R. Lodenkamper, L. J. Lembo, J. C. Brock, and M. C. Wu, "Characterization of a coherent optical RF channelizer based on a diffraction grating," IEEE Trans. Microwave Theory Tech. **49**(10), 1996–2001 (2001).
6. W. Li, N. H. Zhu, and L. X. Wang, "Brillouin-assisted microwave frequency measurement with adjustable measurement range and resolution," Opt. Lett. **37**(2), 166–168 (2012).
7. W. Li, N. H. Zhu, and L. X. Wang, "Reconfigurable Instantaneous Frequency Measurement System Based on Dual-Parallel Mach-Zehnder Modulator," IEEE Photonics J. **4**(2), 427–436 (2012).
8. X. Zou and J. Yao, "An Optical Approach to Microwave Frequency Measurement with Adjustable Measurement Range and Resolution," IEEE Photonics Technol. Lett. **20**(23), 1989–1991 (2008).
9. S. Pan and J. Yao, "Instantaneous microwave frequency measurement using a photonic microwave filter pair," J. Lightwave Technol. **22**, 1437–1439 (2010).
10. D. Shi, J. Wen, S. Zhu, Z. Jia, Z. Shi, M. Li, N. Zhu, and W. Li, "Instantaneous frequency measurement based on non-sliced broadband optical source," Opt. Commun. **458**, 124758 (2020).
11. B. Zhu, W. Zhang, S. Pan, and J. Yao, "High-Sensitivity Instantaneous Microwave Frequency Measurement Based on a Silicon Photonic Integrated Fano Resonator," J. Lightwave Technol. **37**(11), 2527–2533 (2019).
12. X. Zou, S. Xu, S. Li, and W. Zou, "Optimization of the Brillouin instantaneous frequency measurement using convolutional neural networks," Opt. Lett. **44**(23), 5723–5726 (2019).
13. Y. Zhou, F. Zhang, J. Shi, and S. Pan, "Deep neural network-assisted high accuracy microwave instantaneous frequency measurement with a photonic scanning receiver," Opt. Lett. **45**(11), 3038–3041 (2020).
14. X. Xue, X. Zheng, H. Zhang, and B. Zhou, "Widely tunable single-bandpass microwave photonic filter employing a non-sliced broadband optical source," Opt. Express **19**(19), 18423–18429 (2011).
15. M. A. Esmail, W. S. Saif, A. M. Ragheb, and S. A. Alshebeili, "Free space optic channel monitoring using machine learning," Opt. Express **29**(7), 10967–10981 (2021).
16. Z. Zhu and A. K. Nandi, *Automatic Modulation Classification: Principles, Algorithms and Applications* (John Wiley & Sons, 2015).
17. S. Rani, P. C. Biswas, M. A. Hossain, M. R. Islam, and J. Canning, "Polynomial regression of multiple sensing variables for high-performance smartphone colorimeter," OSA Continuum **4**(2), 374–384 (2021).
18. W. S. Saif, A. M. Ragheb, T. A. Alshawi, and S. A. Alshebeili, "Optical Performance Monitoring in Mode Division Multiplexed Optical Networks," J. Lightwave Technol. **39**(2), 491–504 (2021).
19. L. Breiman, "Stacked regressions," Mach. Learn. **24**(1), 49–64 (1996).
20. L. Breiman, "Random forests," Mach Learn **45**(1), 5–32 (2001).
21. T.-J. Ahn, Y. Park, and J. Azana, "Group delay ripple (GDR)measurement for chirped fiber Bragg gratings," in *Proc. LEOS 2007-IEEE Lasers Electro-Opt. Soc. Annu. Meeting Conf.*, 2007, pp. 315–316.